



Contents lists available at ScienceDirect

# Food Science and Human Wellness

journal homepage: <http://www.keaipublishing.com/en/journals/food-science-and-human-wellness>

## Silver nanoparticles on UiO-66 (Zr) metal-organic frameworks for water disinfection application

Hui Chen, Chen Qiu, Yiran Jiang, Xinyu Liao, Dan Wu, Mofei Shen, Tian Ding\*

College of Biosystems Engineering and Food Science, Zhejiang University, Hangzhou 310058, China

### ARTICLE INFO

#### Article history:

Received 13 August 2020

Received in revised form 27 September 2020

Accepted 5 November 2020

Available Online 22 November 2021

#### Keywords:

Metal-organic framework

Silver nanoparticles

Antibacterial effects

Water disinfection

### ABSTRACT

Drinking water disinfection is an essential process to assure public health all over the world. In this study, silver nanoparticles (AgNPs) on UiO-66 (Zr) Metal-Organic Frameworks (Ag@UiO-66) is proposed as a potential water disinfection strategy. AgNPs are synthesized using polyvinyl pyrrolidone (PVP) as stabilizing agent, and sodium borohydride as reducing agent are subsequently embedded on UiO-66, a high-stability organometallic framework. The effect of premixing time, reaction time and reactant concentration on the loading rate of AgNPs on UiO-66 was investigated. The maximum load rate of AgNPs on UiO-66 could reach 13% when the premixing time is 3 h, the reaction time is 45 min and the concentration of AgNO<sub>3</sub> is 10 µg/mL. The formation of AgNPs loaded on UiO-66 was observed and confirmed with ultraviolet and visible spectrophotometry (UV-Vis), scanning electron microscopy (SEM), infrared emission spectroscopy (IES) and X-ray diffraction (XRD) analysis. Ag@UiO-66 exhibited strong antibacterial activity against both Gram-negative *Escherichia coli* and Gram-positive *Staphylococcus aureus*, with minimum inhibitory concentrations (MIC) of 64 and 128 µg/mL, respectively. The germicidal efficacy of Ag@UiO-66 enhanced significantly as the temperature rose from 4 °C to 37 °C. The results indicate that Ag@UiO-66 is potential candidate as a feasible water disinfection material.

© 2022 Beijing Academy of Food Sciences. Publishing services by Elsevier B.V. on behalf of KeAi Communications Co., Ltd. This is an open access article under the CC BY-NC-ND license (<http://creativecommons.org/licenses/by-nc-nd/4.0/>).

### 1. Introduction

Foodborne microbial contamination in water has become an urgent challenge to public health all over the world [1-3]. The bacteria that pollute water are mainly intestinal bacteria (*Streptococcus faecalis*, *Clostridium*, etc.) and other pathogenic bacteria (*Vibrio cholerae*, *S. aureus*, etc.). Diseases caused by bacteria in water occur frequently, especially in developing countries. Currently, water disinfection technologies mainly includes physical and chemical methods. Physical methods are using physical energy to destroy the aggregation of bacteria or the disintegration and denaturation

of bacterial protein, so as to achieve the purpose of drinking water disinfection, such as ultraviolet (UV) and ultrasound [4,5]. Chemical techniques use liquid or gaseous chemical agents to penetrate into the body of bacteria, through violent oxidation reaction, so as to make the bacteria undergo destructive degradation and achieve drinking water disinfection, such as ozone, chlorination, etc. [6,7]. However, the sterilization effect of physical method is limited in a short time, and chemical methods may produce harmful by-products [8]. Therefore, achieving efficient disinfection of water is currently an important research object.

Silver has been used to treat various bacterial infections [9-15] in the form of metallic silver, silver nitrate and silver sulfadiazine. In recent years, with the development of nanotechnology and materials science, silver nanoparticles (AgNPs) with a large surface volume ratio and special crystallographic surface structure, have been widely used for the decontamination of a range of microorganisms with high bactericidal efficacy and low cytotoxicity [16,17]. The antimicrobial efficacy of AgNPs is highly dependent on particle sizes [18]: the

\* Corresponding author at: College of Biosystems Engineering and Food Science, Zhejiang University, Hangzhou, Zhejiang 310058, China.

E-mail address: [tding@zju.edu.cn](mailto:tding@zju.edu.cn) (T. Ding)

Peer review under responsibility of KeAi Communications Co., Ltd.



larger the particle size of silver particles is, the smaller the relative contact area between them and microorganisms is, and the lower their antibacterial ability is. AgNPs in solutions with a high electrolyte are found to aggregate into a mass, which significantly impedes its antibacterial capability [19].

For this reason, suitable dispersants have been proposed in some studies, among which polyvinylpyrrolidone (PVP) is considered a promising one. PVP could efficiently prevent AgNPs from growing and agglomerating. For silver particles with a diameter of less than 50 nm, the coordination of silver and nitrogen atom in PVP plays a protective role against condensation [20,21]. Although the addition of suitable dispersants enhances the stability of AgNPs in dark conditions, AgNPs tend to readily transform in various aqueous environments, causing changes to their properties and antibacterial ability [22].

UiO-66 is a kind of zirconium-based metal-organic framework (Zr-MOF) with advantages of excellent stability, large specific surface area and low toxicity, and thus considered to have a wide range of application scenarios, especially as a carrier of metal nanoparticles [23]. Previous studies have successfully loaded with gold nanoparticles (AuNPs) and palladium nanoparticles (PdNPs) onto UiO-66 and found that these materials were highly stable towards light and heat [24,25]. Therefore, it seems to be a feasible act to embed heavy metal nanoparticles on UiO-66.

This study aims to synthesize a kind of AgNPs particles loaded on UiO-66 (Ag@UiO-66) with PVP as the dispersant. The optimization of various parameters was conducted for achieving maximum loading rate of AgNPs. In addition, the characterization of Ag@UiO-66 were analyzed with scanning electron microscopy (SEM), infrared emission spectroscopy (IES) and X-ray diffraction (XRD). The inactivation efficacy of Ag@UiO-66 was explored in Gram-negative bacteria strain (*Escherichia coli*) and Gram-positive bacteria strain (*S. aureus*) according to minimal inhibitory concentration (MIC) and bactericidal time-kill profiles. Ag@UiO-66 with efficient antibacterial activity can serve as a potential treatment for water decontamination.

## 2. Materials and methods

### 2.1 Materials

AgNO<sub>3</sub> was obtained from Sinopharm Chemical Reagent Co., Ltd. (Beijing, China). Mueller-Hinton broth (MHB), Nutritious broth (NB), Plate count agar (PCA), Baird-Parker RPF Agar, Eosin-methylene blue medium (EMB) and Egg-Yolk Tellurite Emulsion were all purchased from Hope Bio-Technology Co., Ltd. (Qingdao, China). Resazurin sodium salt (90%) was purchased from Adamas Reagent Co., Ltd. (Basel, Switzerland). Polyvinylpyrrolidone, NaBH<sub>4</sub>, ZrCl<sub>4</sub> and *N,N'*-dimethylformamide (DMF) were purchased from Sinopharm Chemical Reagent Co., Ltd. (Beijing, China).

### 2.2 Synthesis of UiO-66

ZrCl<sub>4</sub> (0.800 g) and 1,4-phthalic acid (H<sub>2</sub>BDC) (0.115 g) were dissolved in DMF (40 mL) mixed with acetic acid (1.726 mL) for

the standard synthesis of Zr-BDC MOF (at 25 °C). The mixture was then placed in a preheated oven at 120 °C for 24 h to crystallize under static condition [23]. After cooling down to 25 °C in air, the mixture was separated centrifugally and the solid was collected, subsequently washed with DMF repeatedly and air dried at 25 °C. The UiO-66 should be soaked in alcohol for 24 h for activation before using.

### 2.3 Synthesis of AgNPs

PVP (0.3 g) and AgNO<sub>3</sub> (34 mg) were mixed thoroughly in water (20 mL). NaBH<sub>4</sub> was subsequently added, dropwise, to the mixed solution continuously for 2 h (5 mL/h, 10 mL in total). The solution was stored in a brown flask at low temperature (4 °C). All operations are done in dark conditions.

### 2.4 Synthesis of Ag@UiO-66, the measure the loading rate of AgNPs and the effect of reaction parameters

The procedure for synthesis of Ag@UiO-66 was exhibited in Fig. 1. Specifically, UiO-66 (113 mg) and AgNO<sub>3</sub> (34 mg) were mixed in water (10 mL) and stirred with a magnetic stirrer for 3 h at 100 r/min. PVP solution (10 mL, 3.00%) was then added to the mixed solution. NaBH<sub>4</sub> was further added, dropwise by a quantitative syringe, to the mixed solution continuously for 2 h (5 mL/h, 10 mL in total) during which the mixture is stirred by a magnetic stirrer at 100 r/min. The pellet was washed with water and ethanol for three times, respectively, subsequently dried in a vacuum oven, and the solid was collected. All operations were performed in dark conditions at 4 °C.

The loading rate of silver nanoparticles on UiO-66 was defined as the mass of silver in the mass of unit sample and was determined by inductively coupled plasma mass spectrometry (ICP-MS, NexION 300XX, PerkinElmer, MA). Briefly, Ag@UiO-66 (2.00 mg) is digested by nitric acid at 80 °C for 1 h. The digested mixture is replenished by water to reach a volume of 10 mL, which was used for the analysis of ICP-MS. The parameters for the formation of Ag@UiO-66 included the amount of silver nitrate (34, 68, 102, 136, 170 mg), the premixing time (1, 2, 3, 4, 5 h) and the addition speed of NaBH<sub>4</sub> (5, 6.66, 10, 13.3, 20, 40 mL/h, the corresponding total duration is 2 h, 1.5 h, 1 h, 45 min, 30 min, 15 min).

### 2.5 Ultraviolet and visible spectrophotometry (UV-Vis) spectroscopy for characteristics assay of AgNPs

The UV-Vis spectrum of AgNPs was measured by a UV-Vis spectrometer (UV-2550, Shimadzu, Tokyo, Japan) in the range of 200–800 nm at a spectral resolution of 1 nm inside a 1-cm-path-length quartz cuvette to verify the successful synthesis of AgNPs.

### 2.6 Fourier transform infrared spectroscopy for characteristic assay of UiO-66

The UiO-66 powder was mixed (1:100, *m/m*) with KBr pellets. The Fourier transform infrared (FTIR) spectrum was measured with a resolution of 4 cm<sup>-1</sup> in the scanning range of 4 000 cm<sup>-1</sup> to 400 cm<sup>-1</sup> by using the FTIR spectrophotometer (Nicolet IN10, Thermo Fisher Scientific Inc., USA) to investigate the related functional groups so as to verify the successful synthesis of UiO-66.

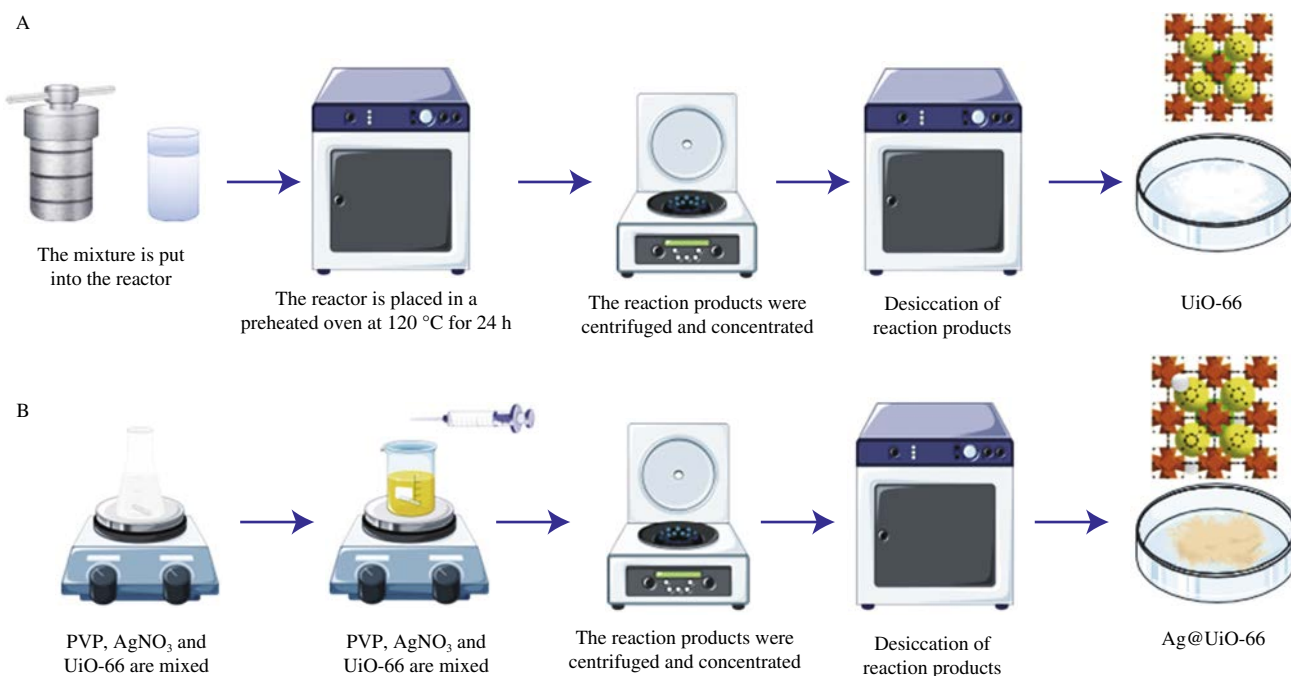


**Fig. 1** Synthesis steps of UiO-66 (A) and Ag@UiO-66 (B).

### 2.7 XRD for characteristics assay of UiO-66 and Ag@UiO-66

The chemical states and surface atomic compositions of UiO-66 and Ag@UiO-66 were identified by the XRD spectra obtained using an X-ray diffractometer (X'Pert PRO MRD/XL, Panalytical., Netherlands) with the CuK- $\alpha$  radiation monochromatic filter at 40 kV and 30 mA. At 25 °C, the diffraction intensity was recorded in the range of 5°–90° at a scanning rate of 1(°)/min. The preparation method of the test sample was the same as that used for FTIR analysis.

### 2.8 SEM and energy dispersive spectrometer (EDS)

The morphology of UiO-66 and Ag@UiO-66 was determined and observed by a scanning electron microscope (GeminiSEM 300, CARL ZEISS Inc., Dublin, CA) after being coated with gold-palladium in ion sputter for 5 min. The mixture of bacteria and Ag@UiO-66 after being placed in a shaking bed for 24 h was washed 3 times in phosphate buffer (0.1 mol/L, pH 7.0) for 15 min and dehydrated under the infrared light before their EDS pictures were taken using the energy dispersive spectrometer combined.

### 2.9 Culture of bacteria and preparation of bacterial suspension

*Escherichia coli* O157:H7 (*E. coli* ATCC 35150) and *Staphylococcus aureus* (*S. aureus* ATCC 25923) were selected as the representatives of Gram-negative and Gram-positive pathogenic bacteria, respectively. The bacterial glycerol stocks were recovered by streaking on the Eosin-Methylene blue agar for *E. coli* and egg-yolk tellurite agar for *S. aureus*, followed by incubation at 37 °C for 24 h. One single colony was transferred into the nutrient broth (NB) for the following 24 h incubation at 180 r/min and 37 °C. The

obtained suspension was centrifuged (6 000 r/min, 8 min, 4 °C) and washed three times with sterile saline solution. The final concentration of both *E. coli* and *S. aureus* was approximate 10<sup>9</sup> CFU/mL.

### 2.10 Minimum inhibitory concentration assays and bactericidal time-kill profiles

Minimum inhibitory concentration (MIC) assays were conducted according to the Performance Standards for Antimicrobial Susceptibility Testing established by Clinical and Laboratory Standards Institute (CLSI). The bacterial suspension was adjusted to 0.5 McFarland turbidity (~10<sup>8</sup> CFU/mL) and further diluted with Mueller-Hinton Broth (MHB) to achieve a concentration of around 10<sup>6</sup> CFU/mL. Then, MHB (100  $\mu$ L) and bacterial suspension (100  $\mu$ L) were added into rows A, B, E and F (Fig. 2). In the two rows of C and D, we added different concentrations of Ag@UiO-66 diluted in MHB, which from microplates numbered 1 to 12 were 2 048, 1 024, 512, 256  $\mu$ g/mL, etc. while the amount of bacterial suspension remained unchanged. In rows G and H, all the microplates were filled with 100  $\mu$ L MHB and 100  $\mu$ L 0.885% sterile saline solution. The plate was sealed with parafilm to avoid evaporation loss. After incubation at 37 °C for 24 h, sodium resazurin (10  $\mu$ L, 0.01%, *m/V*) was added to each microplate and incubated at 37 °C for 2 h. Changes in color from blue to pink were considered to be growth (i.e., positive growth), while no changes were considered to have no significant growth (i.e., negative growth) [26]. MIC referred to the lowest concentration that can completely inhibit the growth of bacteria.

The bactericidal curves for *E. coli* and *S. aureus* at different temperatures (4, 25 and 37 °C) was determined by plate count method. The treated samples (1 mL) was serially diluted with 0.85% sterile saline solution. The appropriate dilution was then spread on the plate count agar (PCA), subsequently by the incubation at 37 °C

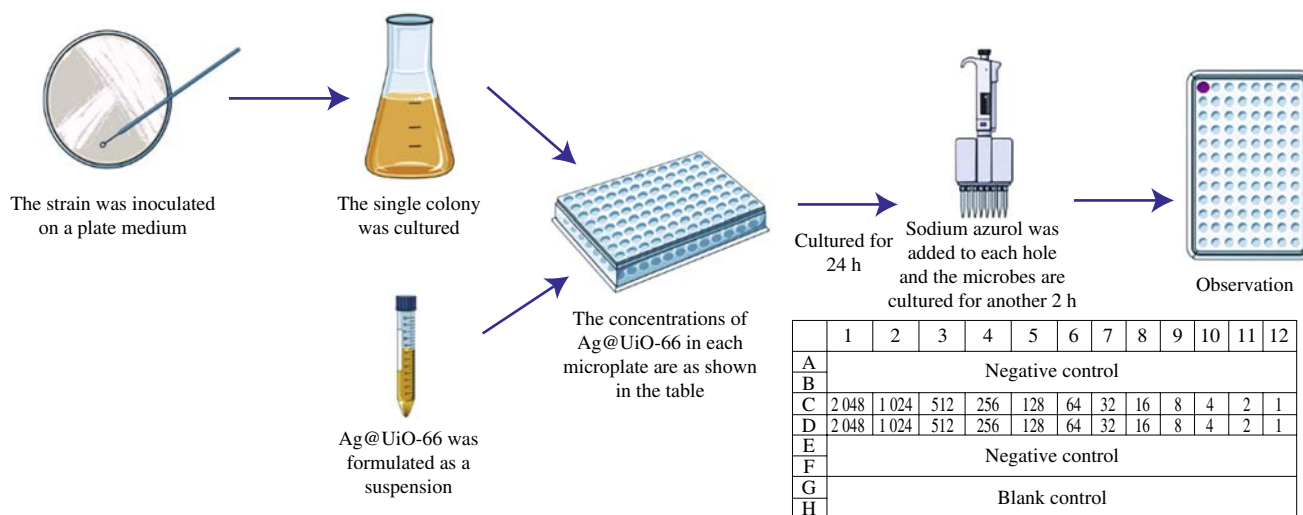


Fig. 2 Experimental procedure of MIC.

for 24 h under atmospheric conditions. The bacterial suspensions mixed with different concentrations of Ag@UiO-66 were incubated in a shaking bed at a speed of 150 r/min. For *S. aureus* at all three temperatures, 100  $\mu$ L was taken out regularly from the mixture every 6 h and the plate counting method was used for colony count. For *E. coli* at 4  $^{\circ}$ C and 25  $^{\circ}$ C, the sample was collected every 12 h, while at 37  $^{\circ}$ C, the time interval of sampling was set at 3 h.

### 2.11 Zeta potential measurement

Zeta potentials of *S. aureus*, *E. coli*, UiO-66 and Ag@UiO-66 were measured using a dynamic light scattering instrument equipped with a zeta DTS1060 cell (Zetasizer Nano ZS, Malvern Instruments, Ltd., Malvern, UK) after the samples were made into suspension in 0.85% sterile saline solution. The same volume of 0.85% sterile saline solution was used as the control. After 2-min balance, all measurements were conducted in triplicate at room temperature ((25  $\pm$  2)  $^{\circ}$ C).

### 2.12 Statistical analysis

All operations were repeated in triplicate. Microsoft Office Excel 2019 (Microsoft Inc., USA) was used to collect and organize data. Spectrum analysis was performed using OriginLab (Version 8.0; Microsoft Software Inc., Northampton, MA). R (Version 3.6.3) and ggplot2 package were used in data analysis and visualization. In this paper, the data is expressed in the form of mean  $\pm$  standard deviation (SD). Statistical significance will be declared when  $P < 0.05$ .

## 3. Results and discussion

### 3.1 Effects of reaction parameters on loading rate of AgNPs on UiO-66

Fig. 3 shows the change of loading rate of AgNPs on UiO-66 under different conditions. The maximum loading rate could reach

17.7% when the reaction time is 45 min, the premixing time is 3 h, and the concentration of silver nitrate is 10  $\mu$ g/mL.

Premixing time is a main factor affecting the status of silver ions before reaction. Adequate premixing time is needed to make sure that silver ions can be embed on UiO-66. However, excessive time contributes to the deterioration of silver ions. Therefore, a U-shape curve is shown when considering the effect of premixing time on loading rate of AgNPs on UiO-66.

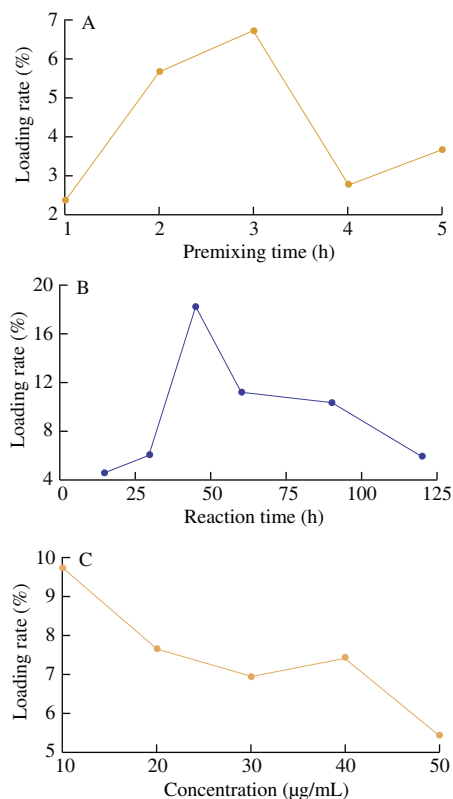


Fig. 3 Effect of reaction parameters on the loading rate of AgNPs on UiO-66. (A) Loading rates under different premixing times, (B) loading rates under different reaction times, (C) loading rates using different concentrations of AgNO<sub>3</sub>.

The reaction time is controlled by the dripping speed of  $\text{NaBH}_4$ , the reducing agent in the reaction of formation of AgNPs. The rise of the dripping speed of  $\text{NaBH}_4$  will increase its local concentration, making the silver particles synthesized larger. As a result, the generated silver can not be loaded on UiO-66 effectively. Excessively long reaction time would contribute to the deterioration of silver ions as is stated. Therefore, the loading rate first increased and then decreased as the extension of reaction time.

In the synthesis process, the loading rate decreases as the concentration of  $\text{AgNO}_3$  increases because the silver particles produced would then be larger and harder to be loaded on UiO-66.

### 3.2 Characterization of AgNPs, UiO-66 and Ag@UiO-66

Fig. 4 exhibits the UV-Vis spectrum of AgNPs synthesized in this study. It is found that the highest absorption peak was at around wavelength of 400 nm, which indicates that the PVP method is successful in preparing AgNPs, given that previous study has proved that a absorption peak at around 400 nm is a feature of AgNPs [26]. FTIR spectroscopy and XRD analysis of UiO-66 was shown in Fig. 5. The characteristic peaks of UiO-66 were observed at 3 397, 2 778, 1 654, and 1 391  $\text{cm}^{-1}$ . The broad band at 3 397  $\text{cm}^{-1}$  in UiO-66 corresponds to the —OH vibration of the monomer unit [27]. Due to the strong tensile vibration of the hydroxyl functional group, the broad peak is observed. The peak at 2 778  $\text{cm}^{-1}$  corresponds to

C—H stretching, the peak at 1 654  $\text{cm}^{-1}$  corresponds to C—O stretching, and the peak at 1 391  $\text{cm}^{-1}$  corresponds to symmetric vibration of the C—H bond [28]. In addition, the XRD results also shows that the UiO-66 diffraction peak position, height, and width were basically consistent with previous literatures [29,30]. Both FTIR and XRD results prove the successful synthesis of the UiO-66 in this study.

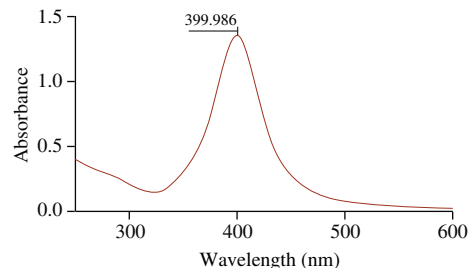


Fig. 4 UV-Vis spectra of AgNPs synthesized using PVP as stabilizing agent.

The morphology of UiO-66 synthesized in this study showed in a hexahedral shape (Fig. 6), in consistence with previous study [29]. The characteristic peak for silver ( $2\theta - 38^\circ$ ) implies that the formation of AgNPs on UiO-66. After loaded with AgNPs, the surface structure of the organometallic material can be seen in its SEM image. In short, both XRD and SEM results confirm that the AgNPs successfully loaded on UiO-66.

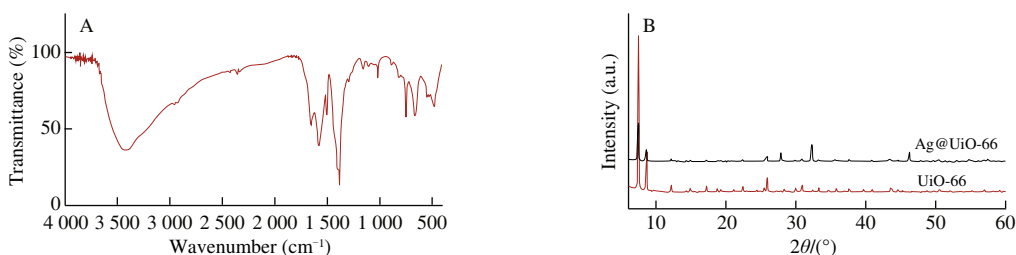


Fig. 5 FTIR spectra of UiO-66 (A) and XRD spectra of UiO-66 and Ag@UiO-66 (B).

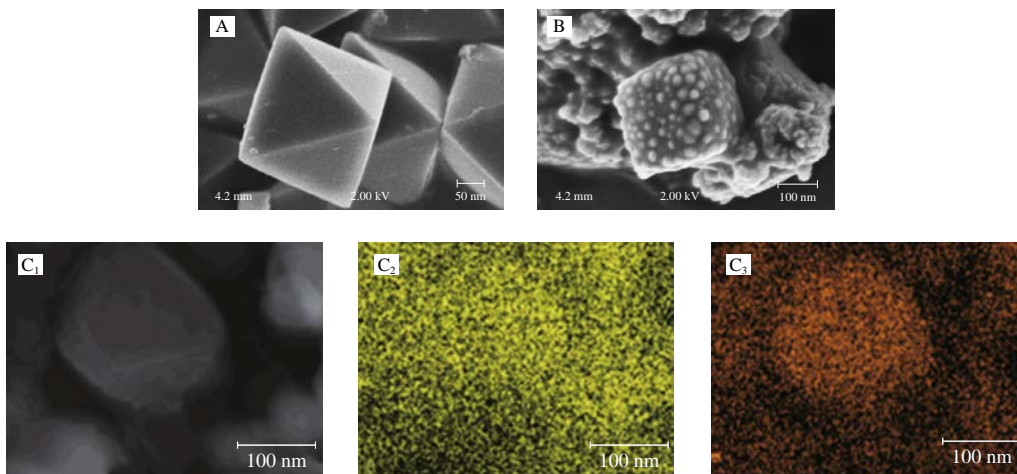


Fig. 6 SEM of UiO-66, Ag@UiO-66 and EDS images of UiO-66, Ag@UiO-66 and Ag@UiO-66 absorbed on bacteria. (A) SEM image of UiO-66; (B) SEM image of Ag@UiO-66; (C) EDS images of Ag@UiO-66; (D) EDS images of Ag@UiO-66 absorbed on *S. aureus*; (E) EDS images of Ag@UiO-66 absorbed on *E. coli*.

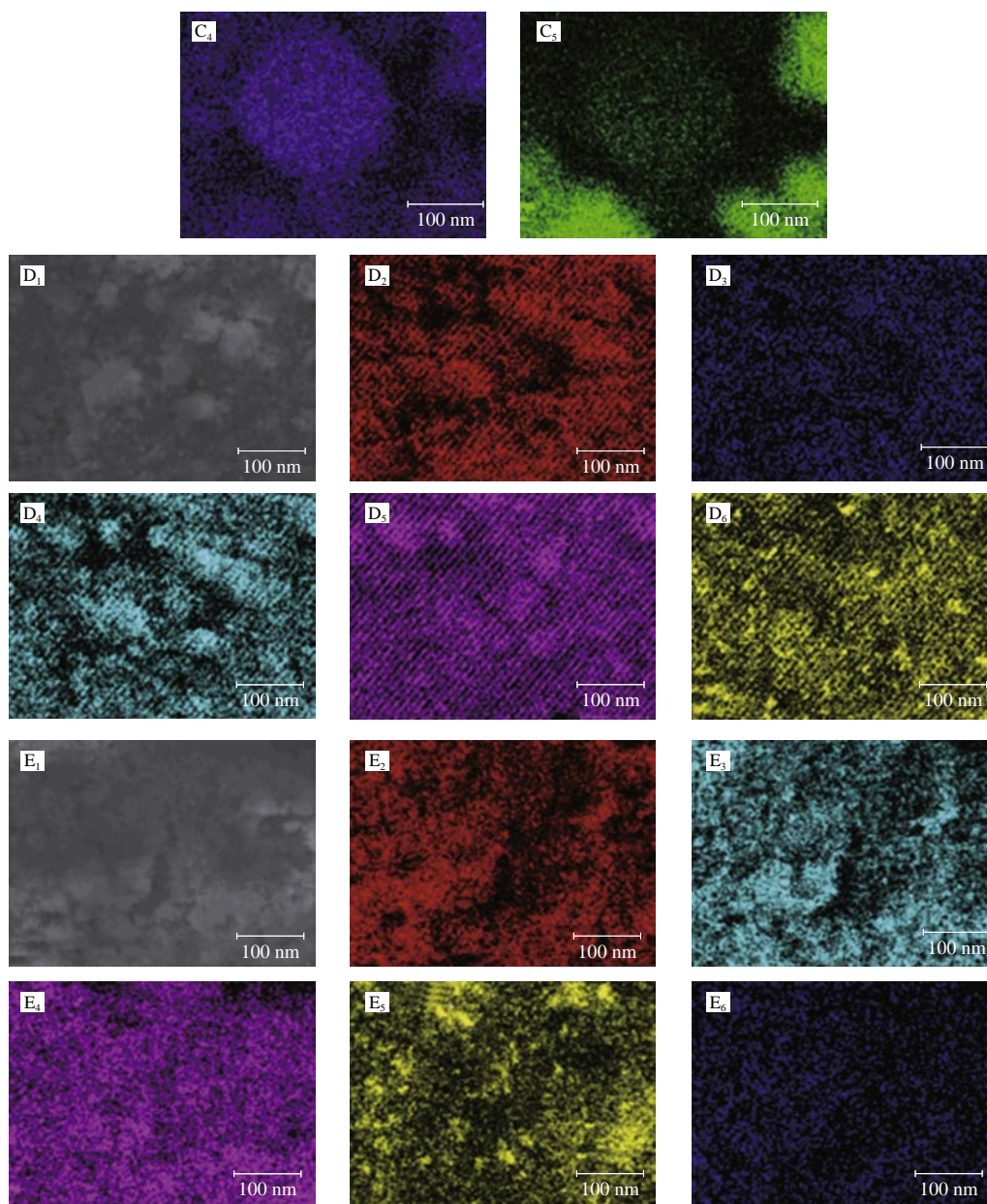


Fig. 6 (Continued)

### 3.3 Antibacterial efficacy and mechanisms of Ag@UiO-66

Ag@UiO-66 absorbed on and covered the surface of bacteria after their mixing (Fig. 6). EDS images of Ag@UiO-66 absorbed on *S. aureus* and *E. coli* illustrates that AgNPs embedded on UiO-66 are thus able to come into contact with bacteria and function as antibacterial agents.

Antibacterial activity of Ag@UiO-66 is determined by MIC assay (Fig. 7). In rows A, B, E and F, all the microplates added with MHB and bacterial suspension were pink, indicating that microorganism can grow normally. In rows G and H, all the microplates filled with MHB and saline solution were blue, indicating that there are no living bacteria in these microplates. For *E. coli* and *S. aureus*, the MIC of Ag@UiO-66 are 64 and 128  $\mu\text{g}/\text{mL}$  as is shown in rows C and D, respectively.



Fig. 7 (A) MIC assay of Ag@UiO-66 on *E. coli*, (B) MIC assay of Ag@UiO-66 on *S. aureus*.

Zeta-potential analysis shows that the surface of UiO-66 is negatively charged ( $P < 0.05$ , Table 1), which explains its binding to positively charged AgNPs ( $P < 0.01$ ). The negative charge on the surface of bacteria ( $P < 0.01$ ) and the positive charge on the surface of Ag@UiO-66 ( $P < 0.01$ ) explain the adsorption of the latter on the former. In the solution, under the synergistic action of oxygen and proton, AgNPs release silver ions ( $\text{Ag}^+$ ) to play an antibacterial role. The electrostatic adsorption between AgNPs and bacteria makes it easier for  $\text{Ag}^+$  released from AgNPs to enter bacteria. Silver ions can affect various biochemical reactions in bacteria through chemical interaction with thiohydrogen groups ( $-\text{SH}$ ) to change the activity of enzymes in bacteria, and then cause death to bacteria.

**Table 1**  
Zeta-potentials on the surfaces.

Item	Zeta-potential on the surface (mV)	P-value
UiO-66	$-0.32 \pm 0.16^{**}$	0.036
Ag@UiO-66	$7.83 \pm 2.63^{**}$	0.005
<i>S. aureus</i>	$-30.56 \pm 1.59^{***}$	$< 0.001$
<i>E. coli</i>	$-4.12 \pm 2.17^{**}$	0.003

Note: \*  $P < 0.05$ ; \*\*  $P < 0.01$ ; \*\*\*  $P < 0.001$ .

The time-killing curves (Fig. 8) show the germicidal efficacy of different concentrations of Ag@UiO-66 against *E. coli* and *S. aureus*. Ag@UiO-66 performed a germicidal efficacy for a long period of time at all three temperatures, while the curves show disparate features. In general, the higher the incubation temperature is, the faster the bacteria are killed by Ag@UiO-66. For example, in the *E. coli* group treated at 4 °C, *E. coli* decreased by 1 (lg(CFU/mL)) in the first 6 h, and more slowly in the following hours, but at 25 °C, the reduction is 1 (lg(CFU/mL)) every 6 h, and at 37 °C, the reduction is 3 (lg(CFU/mL)) in the first 3 h. Similar phenomenon appears in the *S. aureus* group. However, increasing the concentration of Ag@UiO-66 does not seem to significantly enhance the germicidal efficacy. Previous studies have shown that when the temperature increases, the

permeability of bacterial cell wall and cell membrane tend to increase, which may make bacteria more vulnerable to substances entering the cell [31,32].

When comparing the Gram-negative and Gram-positive bacteria, the results are not the same. Basically, *E. coli* are more susceptible to Ag@UiO-66. For example, at 37 °C, all *E. coli* are killed in the first 6 h, while the reduction of *S. aureus* is about 3 (lg(CFU/mL)). At 4 and 25 °C, the curves of *E. coli* are also steeper than that of *S. aureus*. The cell structure of bacteria can also explain to some extent that Ag@UiO-66 have different bactericidal effects on Gram-negative bacteria (represented by *E. coli*) and Gram-positive bacteria (represented by *S. aureus*). As the cell wall is thicker, Gram-positive bacteria may be more difficult to be inactivated, which is confirmed in our results.

At the same time, it should not neglect that increasing the concentration of Ag@UiO-66 posed limited effect on improving the bactericidal performance. The reason might be that for the number of bacteria we use, Ag@UiO-66 at a concentration of 128  $\mu\text{g/mL}$  has well covered the bacteria, so the promotion of increasing the concentration of it is limited for this process.

Primary step in water treatment was mainly to remove the suspended substances, and settling method was commonly used, during which bacteriobacteria is likely to proliferate. The utilization of this technology can reduce the risk of bacterial contamination because of its bactericidal efficacy and shorten the settling time because of its adsorption performance. Although this application needs to be verified further, the prospect is worth looking forward to. Since the stability of the structure of UiO-66 is stable in water as stated [33], AgNPs potentially desorbed from UiO-66 could be the main risk when the material is utilized in tap water disinfection. Studies on the toxicity of AgNPs can interfere with stem spermatogonium by slowing its proliferation at a concentration of 10  $\mu\text{g/mL}$  [34]. The premise for this is that the nanoparticles exists in extracellular fluid and functions continuously. For drinking water, in the proposition, the concentration would be much lower even if some

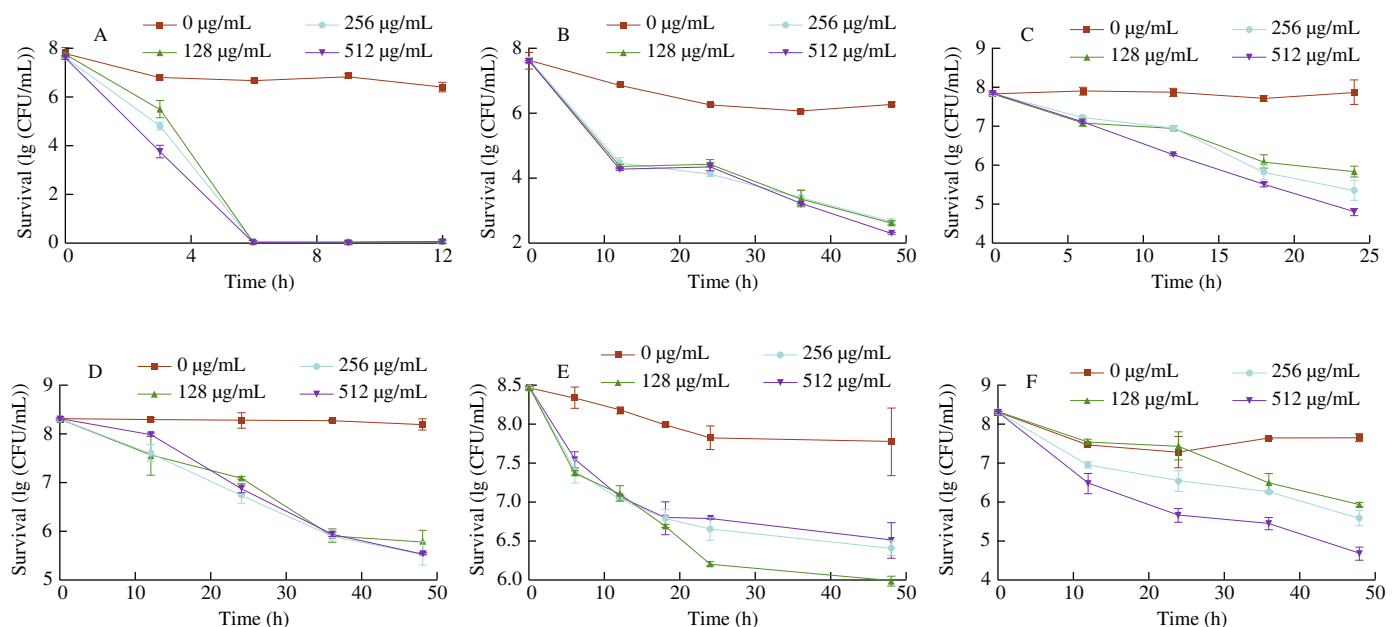


**Fig. 8** Killing curve of Ag@UiO-66 on *E. coli* (A, C, E) and *S. aureus* (B, D, F) at 37 °C (A–B), 25 °C (C–D) and 4 °C (E–F).

AgNPs desorbed from UiO-66. Although we have made preliminary predictions about the safety of this material, more research is still needed to confirm its safety before it can be utilized.

#### 4. Conclusions

Our research proposed and synthesized a kind of AgNPs loaded on metal-organic framework UiO-66 (Ag@UiO-66). Its structure and characteristics were further analyzed by FTIR, XRD, SEM and its antibacterial effect under different conditions was explored as well. Embedded on MOFs, AgNPs may be feasible for the treatment of microbial contamination in water environment with extended duration. Our research also points out the direction for future research: it is necessary to reevaluate the performance of Ag@UiO-66 in actual polluted water system. Also, the stability and safety of Ag@UiO-66 needs more research to explore.

#### Declaration of competing interest

The authors declare no conflicts of interests.

#### Acknowledgement

This work was supported by the Student Research Training Program (SRTP) of Zhejiang University [Y201931165]. The funding agency had no role in study design, data collection, interpretation and analysis, decision to publish, or preparation of the manuscript.

#### References

- [1] S. Dwivedi, S. Mishra, R.D. Tripathi, Ganga water pollution: a potential health threat to inhabitants of Ganga basin, *Environ. Int.* 117 (2018) 327-338. <https://doi.org/10.1016/j.envint.2018.05.015>.
- [2] V. Girardi, K.D. Mena, S.M. Albino, et al., Microbial risk assessment in recreational freshwaters from southern Brazil, *Sci. Total Environ.* 651 (2019) 298-308. <https://doi.org/10.1016/j.scitotenv.2018.09.177>.
- [3] T. Huang, ed., *Water pollution and water quality control of selected Chinese Reservoir Basins*, Springer International Publishing, Cham, (2016) 155-168. <https://doi.org/10.1007/978-3-319-20391-1>.
- [4] T. Nakamura, H. Okawa, R. Hosokawa, et al., The sterilization of suspensions contaminated with microorganisms using ultrasound irradiation, *Jpn. J. Appl. Phys.* 49 (2010) 5. <https://doi.org/10.1143/JJAP.49.07HE11>.
- [5] K. Song, M. Mohseni, F. Taghipour, Application of ultraviolet light-emitting diodes (UV-LEDs) for water disinfection: a review, *Water Res.* 94 (2016) 341-349. <https://doi.org/10.1016/j.watres.2016.03.003>.
- [6] K.K. Jyoti, A.B. Pandit, Ozone and cavitation for water disinfection, *Biochem. Eng. J.* 18 (2004) 9-19. [https://doi.org/10.1016/S1369-703X\(03\)00116-5](https://doi.org/10.1016/S1369-703X(03)00116-5).
- [7] S.D. Richardson, A.D. Thruston, T.V. Caughran, et al., Identification of new drinking water disinfection by-products from ozone, chlorine dioxide, chloramine, and chlorine, *Water Air Soil Poll.* 123 (2000) 95-102. <https://doi.org/10.1023/A:1005265509813>.
- [8] J.P. Scott, D.F. Ollis, Integration of chemical and biological oxidation processes for water treatment: review and recommendations, *Environ. Prog.* 14 (1995) 88-103. <https://doi.org/10.1002/ep.670140212>.
- [9] B.S. Atiyeh, M. Costagliola, S.N. Hayek, et al., Effect of silver on burn wound infection control and healing: review of the literature, *Burns* 33 (2007) 139-148. <https://doi.org/10.1016/j.burns.2006.06.010>.
- [10] T.J. Berger, J.A. Spadaro, S.E. Chapin, et al., Electrically generated silver ions: quantitative effects on bacterial and mammalian cells, *Antimicrob. Agents Chemother.* 9 (1976) 357-358. <https://doi.org/10.1128/aac.9.2.357>.
- [11] K. Dunn, V. Edwards-Jones, The role of Acticoat™ with nanocrystalline silver in the management of burns, *Burns* 30 (2004) S1-S9. [https://doi.org/10.1016/S0305-4179\(04\)90000-9](https://doi.org/10.1016/S0305-4179(04)90000-9).
- [12] C.L. Fox, Silver sulfadiazine - a new topical therapy for pseudomonas in burns: therapy of pseudomonas infection in burns, *Arch. Surg.* 96 (1968) 184-188. <https://doi.org/10.1001/archsurg.1968.01330200022004>.
- [13] H.J. Klasen, A historical review of the use of silver in the treatment of burns. II. Renewed interest for silver, *Burns* 26 (2000) 131-138. [https://doi.org/10.1016/S0305-4179\(99\)00116-3](https://doi.org/10.1016/S0305-4179(99)00116-3).
- [14] T. Maneerung, S. Tokura, R. Rujiravanit, Impregnation of silver nanoparticles into bacterial cellulose for antimicrobial wound dressing, *Carbohydr. Polym.* 72 (2008) 43-51. <https://doi.org/10.1016/j.carbpol.2007.07.025>.
- [15] S. Silver, L.T. Phung, G. Silver, Silver as biocides in burn and wound dressings and bacterial resistance to silver compounds, *J. Ind. Microbiol. Biotechnol.* 33 (2006) 627-634. <https://doi.org/10.1007/s10295-006-0139-7>.
- [16] J.S. Kim, E. Kuk, K.N. Yu, et al., Antimicrobial effects of silver nanoparticles, *Nanomedicine* 3 (2007) 95-101. <https://doi.org/10.1016/j.nano.2006.12.001>.
- [17] J.R. Morones, J.L. Elechiguerra, A. Camacho, et al., The bactericidal effect of silver nanoparticles, *Nanotechnology* 16 (2005) 2346-2353. <https://doi.org/10.1088/0957-4484/16/10/059>.
- [18] O. Choi, K.K. Deng, N.J. Kim, et al., The inhibitory effects of silver nanoparticles, silver ions, and silver chloride colloids on microbial growth, *Water Res.* 42 (2008) 3066-3074. <https://doi.org/10.1016/j.watres.2008.02.021>.
- [19] X. Li, J.J. Lenhart, H.W. Walker, Dissolution-accompanied aggregation kinetics of silver nanoparticles, *Langmuir* 26 (2010) 16690-16698. <https://doi.org/10.1021/la101768n>.
- [20] A. Slistan-Grijalva, R. Herrera-Urbina, J.F. Rivas-Silva, et al., Assessment of growth of silver nanoparticles synthesized from an ethylene glycol-silver nitrate-polyvinylpyrrolidone solution, *Physica E Low Dimens. Syst. Nanostruct.* 25 (2005) 438-448. <https://doi.org/10.1016/j.physe.2004.07.010>.
- [21] T. Tsuji, D.H. Thang, Y. Okazaki, et al., Preparation of silver nanoparticles by laser ablation in polyvinylpyrrolidone solutions, *Appl. Surf. Sci.* 254 (2008) 5224-5230. <https://doi.org/10.1016/j.apsusc.2008.02.048>.
- [22] L. Clement, E.M. Hotze, G.V. Lowry, Environmental transformations of silver nanoparticles: impact on stability and toxicity, *Environ. Sci. Technol.* 46(13) (2012) 6900-6914. <https://doi.org/10.1021/es2037405>.
- [23] J.H. Cavka, S. Jakobsen, U. Olsbye, et al., A new zirconium inorganic building brick forming metal organic frameworks with exceptional stability, *J. Am. Chem. Soc.* 130 (2008) 13850-13851. <https://doi.org/10.1021/ja8057953>.
- [24] W. Dong, C. Feng, L. Zhang, et al., Pd@UiO-66: an efficient catalyst for Suzuki-Miyaura coupling reaction at mild condition, *Catal. Lett.* 146 (2016) 117-125. <https://doi.org/10.1007/s10562-015-1659-4>.
- [25] J. Zhu, P.C. Wang, M. Lu, Selective oxidation of benzyl alcohol under solvent-free condition with gold nanoparticles encapsulated in metal-organic framework, *Appl. Catal. A-Gen.* 477 (2014) 125-131. <https://doi.org/10.1016/j.apcata.2014.03.013>.
- [26] Y. Shao, C. Wu, T. Wu, et al., Green synthesis of sodium alginate-silver nanoparticles and their antibacterial activity, *Int. J. Biol. Macromol.* 111 (2018) 1281-1292. <https://doi.org/10.1016/j.ijbiomac.2018.01.012>.
- [27] E. Virmani, J.M. Rotter, A. Mähringer, et al., On-surface synthesis of highly oriented thin metal-organic framework films through vapor-assisted conversion, *J. Am. Chem. Soc.* 140 (2018) 4812-4819. <https://doi.org/10.1021/jacs.7b08174>.
- [28] M. Tammer, G. Sokrates, Infrared and Raman characteristic group frequencies: tables and charts, *Colloid Polym. Sci.* 283 (2004) 235. <https://doi.org/10.1007/s00396-004-1164-6>.
- [29] Y.X. Li, ZY. Wei, L. Liu, et al., Ag nanoparticles supported on UiO-66 for selective oxidation of styrene, *Inorg. Chem. Commun.* 88 (2018) 47-50. <https://doi.org/10.1016/j.inoche.2017.12.011>.
- [30] Y. Luan, Y. Qi, H. Gao, et al., A general post-synthetic modification approach of amino-tagged metal-organic frameworks to access efficient catalysts for the Knoevenagel condensation reaction, *J. Mater. Chem. A* 3 (2015) 17320-17331. <https://doi.org/10.1039/C5TA00816F>.
- [31] C.W.M. Haest, J. De Gier, J.A.F. Op Den Kamp, et al., Changes in permeability of *Staphylococcus aureus* and derived liposomes with varying lipid composition, *Biochim. Biophys. Acta Biomembr.* 255 (1972) 720-733. [https://doi.org/10.1016/0005-2736\(72\)90385-9](https://doi.org/10.1016/0005-2736(72)90385-9).
- [32] C.W.M. Haest, J. De Gier, G.A. Van Es, et al., Fragility of the permeability barrier of *Escherichia coli*, *Biochim. Biophys. Acta Biomembr.* 288 (1972) 43-53. [https://doi.org/10.1016/0005-2736\(72\)90221-0](https://doi.org/10.1016/0005-2736(72)90221-0).
- [33] M. Kandiah, M.H. Nilsen, S. Usseglio, et al., Synthesis and stability of tagged UiO-66 Zr-MOFs, *Chem. Mater.* 22 (2010) 6632-6640. <https://doi.org/10.1021/cm102601v>.
- [34] L.K. Braydich-Stolle, B. Lucas, A. Schrand, et al., Silver nanoparticles disrupt GDNF/Fyn kinase signaling in spermatogonial stem cells, *Toxicol. Sci.* 116 (2010) 577-589. <https://doi.org/10.1093/toxsci/kfq148>.